Three-dimensional band structure of highly metallic $Na_{0.8}WO_3$ by angle-resolved photoemission spectroscopy

Satyabrata Raj,[1,2,*] Anirban Chakraborty,[3] Debraj Choudhury,[3] Takafumi Sato,[1] Takashi Takahashi,[1,4] Priya Mahadevan,[5] Jun Fujii,[6] Ivana Vobornik,[6] and D. D. Sarma[3,7,†]

[1]*Department of Physics, Tohoku University, Sendai 980-8578, Japan*

[2]*Indian Institute of Science Education and Research, Salt Lake, Kolkata 700106, India*

[3]*Solid State and Structural Chemistry Unit, Indian Institute of Science, Bangalore 560 012, India*

[4]*WPI Research Center, Advanced Institute for Materials Research, Tohoku University, Sendai 980-8577, Japan*

[5]*S. N. Bose National Centre for Basic Sciences, JD Block, Sector 3, Salt Lake, Kolkata 700 098, India*

[6]*TASC National Laboratory, INFM-CNR, SS 14, km 163.5, I-34012 Trieste, Italy*

[7]*Centre for Advanced Materials, Indian Association for the Cultivation of Science, Kolkata 700 032, India*

(Received 17 August 2008; published 22 January 2009)

Three-dimensional electronic structure of highly metallic sodium tungsten bronze, $Na_{0.8}WO_3$, is investigated by high-resolution angle-resolved photoemission spectroscopy. The experimentally determined valence-band structure along the momentum directions both parallel and perpendicular to the surface has been compared with the results of *ab initio* band-structure calculation. The angle-resolved photoemission spectroscopy spectra for different photon energies reveal that possibly the oxygen vacancies in the system are responsible for the evolution of density of states at the top of Γ point in experimental valence band. The band dispersion around $\Gamma(X)$ point leading to an electronlike Fermi surface is well predicted by the band calculation. As we move from bulk-sensitive to more-surface-sensitive photon energy, we found emergence of Fermi surfaces at $X(M)$ and $M(R)$ points similar to the one at $\Gamma(X)$ point, suggesting the reconstruction of surface due to rotation/deformation of WO_6 octahedra.

DOI: 10.1103/PhysRevB.79.035119 PACS number(s): 79.60.−i, 71.30.+h, 71.18.+y

I. INTRODUCTION

Bulk tungsten trioxide, WO_3, is a technologically important ceramic having several potential applications in devices.[1,2] In particular, it shows very interesting optical properties[3] when sodium (Na) is inserted in bulk WO_3 forming the series of sodium tungsten bronzes. Color of Na_xWO_3 crystal changes dramatically as a function of Na concentration (x), showing almost all kinds of colors in visible spectrum. In addition, the metal-insulator transition (MIT) observed as a function of x is one of the most interesting electronic properties in Na_xWO_3. A high metallic conduction is obtained for $x \geq 0.25$, and the system undergoes MIT with decreasing x.[4] Hence the investigation of the electronic structure of Na_xWO_3 is of great interest from both technological and fundamental perspectives.

In addition to the marked influence to the optical and transport properties, the insertion of Na also has a strong effect on the crystal structure. Na_xWO_3 shows a fairly rich phase diagram[5] with increasing x. The crystal structure changes from monoclinic, to orthorhombic, to tetragonal, and finally to cubic with increasing x. For $x \leq 0.4$, variety of structural modifications exist, while for $x \geq 0.5$, Na_xWO_3 is highly metallic with perovskite-type crystal structure. Figure 1(a) shows the crystal structure of $NaWO_3$, where Na^+ ions occupy the center of the cube, while the WO_6 octahedra are located at the cube corners. The octahedral crystal field of the six oxygen neighbors of the W split the W 5*d* bands into triply degenerate t_{2g} and doubly degenerate e_g bands. In Na_xWO_3, the Na 3*s* electrons are transferred into the W 5*d* t_{2g} π^* band, and the system is expected to behave as a metal for any value of x. However, for low concentration of $x \leq 0.25$, the material is insulating and the origin of MIT is likely due to the random distribution of Na^+ ions in the WO_3 lattice.[6] This gives rise to strong disorder effects, which lead to the localization of states at the conduction-band tail, and the system therefore undergoes an MIT for low Na concentration.

Photoemission spectroscopy is one of the most powerful experimental techniques to extract information of electronic structure, and Na_xWO_3 has been the subject of numerous photoemission studies. Unfortunately, the majority of these previous studies are based on angle-integrated photoemission spectroscopy which just determine the spectral density of states, but not the band structure or Fermi surface (FS).[7–10] Very recently, we have carried out high-resolution angle-resolved photoemission spectroscopy (ARPES) on highly metallic and insulating Na_xWO_3 with constant incident photon energy.[6,11,12] These ARPES studies were compared with the pseudopotential band calculation, and few discrepancies have been reported. First, in both the metallic and insulating

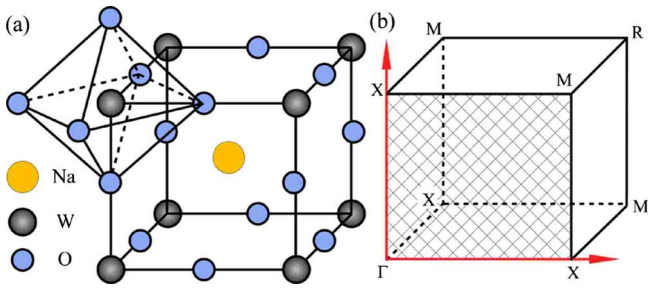

FIG. 1. (Color online) (a) Crystal structure and (b) cubic Brillouin zone showing high-symmetry lines of $NaWO_3$.

regions, the top of the valence band at $\Gamma(X)$ point is not predicted by the band calculation. Second, in insulating region, we found an electronlike remnant FS at $\Gamma(X)$ point whose dispersion agrees well with the band calculation, while similar remnant FSs are also observed at $X(M)$ and $M(R)$ points in contradiction to the band calculation. The evolution of remnant FSs in insulating phase of Na_xWO_3 at other symmetry points is explained by the surface reconstruction. However, it is still unknown whether or not such kind of surface reconstruction exists in the highly metallic Na_xWO_3 surfaces. To understand these issues, a three-dimensional band structure and FS measurements at different bulk and surface-sensitive photon energies on metallic Na_xWO_3 are highly required. Hence a synchrotron-based photon-energy-dependent ARPES measurement is absolutely necessary to clarify these issues.

In this paper, we report high-resolution ARPES measurements on highly metallic $Na_{0.8}WO_3$ with different incident photon energies. The valence-band structure along momentum directions both the parallel and perpendicular to the surface has been established experimentally. We have also carried out *ab initio* band-structure calculations based on the plane-wave pseudopotential method and compared it with experimental results. We found a small finite dispersion of valence-band edge at $\Gamma(X)$ point as a function of photon energy, confirming the essentially three-dimensional nature of the band. The FS shows an electronlike pocket centered at $\Gamma(X)$ point in the Brillouin zone (BZ) [Fig. 1(b)], in good agreement with the band calculation. As we move from bulk-sensitive to more-surface-sensitive photon energy, we found an evidence for the emergence of new FSs at $X(M)$ and $M(R)$ points arising from the surface reconstruction.

II. EXPERIMENTS

Single crystals of $Na_{0.8}WO_3$ were grown by the fused salt electrolysis of Na_2WO_4 and WO_3 as described by Shanks.[13] The electrical resistivity measurement and the Laue diffraction pattern show that the crystals are highly metallic with a single cubic phase. The x value was obtained from the measured lattice parameter, as described by Brown and Banks.[14] High-resolution ARPES measurements were performed with a VG-SCIENTA SES-2002 analyzer. The band structure along the momentum direction parallel to surface ($k_\parallel$) was obtained from the laboratory-based spectrometer at Tohoku University with the He Iα ($h\nu$=21.218 eV) unpolarized resonance line, whereas the band structure along the momentum direction perpendicular to the surface ($k_\perp$) was obtained by varying photon energy from 25–42 eV (sample 1) with a linear horizontal polarization and 49–85 eV (sample 2) with a circular polarization at the low-energy branch of the APE-INFM beam line installed at the Elettra synchrotron, Italy, and BL-28A beam line at Photon Factory (PF), KEK, Japan, respectively. ARPES spectra were measured along both the $k_\parallel$ and $k_\perp$ directions of the high-symmetry $\Gamma(X)$-$X(M)$ line of BZ, as shown in Fig. 1(b). The FS measurements at different photon energies (except for the He-Iα photons) were measured with a linear horizontal (p type) polarization of the Apple II nonperiodical undulator available at the beamline of Elettra. The energy and angular resolutions were set at 5–25 meV and 0.2°, respectively. The measurements for metallic $Na_{0.8}WO_3$ were performed at 14 K and room temperature for laboratory-based and synchrotron-based measurements, respectively, in a vacuum better than 5×10^{-11} Torr. A clean surface of the sample for ARPES measurements was obtained by *in situ* cleaving along (001) surface. The Fermi level (E_F) of the sample was referred to that of a gold film evaporated on the sample substrate.

III. BAND CALCULATIONS

We have performed *ab initio* band-structure calculations for $NaWO_3$ (x=1.0) using projected augmented wave potential[15,16] as implemented in the Vienna *ab initio* simulation package (VASP) code.[17] A k-points mesh of $8\times8\times8$ with lattice constant of 3.86 Å and the generalized gradient approximation (GGA) for the exchange were used for the calculation. We have simulated electron doping (x=0.8) in our calculations by a rigid-band shift of the band structure and the corresponding calculated Fermi surfaces have been compared with the experiment. Since the GGA exchange based calculations have the drawback of underestimating the band gap, we use the scissor operator technique to independently align the calculated valence and conduction-band structure with the experiment.

IV. RESULTS AND DISCUSSION

Figures 2(a) and 2(b) show valence-band ARPES spectra and experimental band structure of highly metallic $Na_{0.8}WO_3$ at 14 K with the He Iα photons measured along $\Gamma(X)$-$X(M)$ direction parallel to surface ($k_\parallel$) in the BZ. In metallic $Na_{0.8}WO_3$, E_F is situated in the conduction band, which lies around 1.5 eV binding energy, whereas the top of the valence band extends up to 3.5 eV indicating a large (2 eV) energy gap. This large energy gap corresponds to the hard band gap observed in insulating WO_3. The pseudopotential band structure for cubic $NaWO_3$ is also presented in Fig. 2(b) for comparison. It is found from the band calculation that the valence band of $Na_{0.8}WO_3$ consists mostly of the O $2p$ states along with a small admixture of bonding W $5d$ e_g states. We found that the top of the valence band, which is less dispersive at 3.5 eV around $\Gamma(X)$ point, is not predicted in the band calculation. Nevertheless, the band around 4.5 eV at $\Gamma(X)$ point, which disperses along $\Gamma(X)$-$X(M)$ direction is in good agreement with the band calculation. We note that the observed discrepancy between the experiment and calculation could be attributed to the possible final-state effects. In this sense, the information of energy bands above the vacuum level would be important, as they constitute the final states in photoemission process. To better characterize this final-state effect, selected incident photon energies are necessary, which can be obtained correctly by other experiments such as inverse photoemission spectroscopy (IPES) and very low-energy electron-diffraction (VLEED) experiment as intensively studied in other system.[18–20]

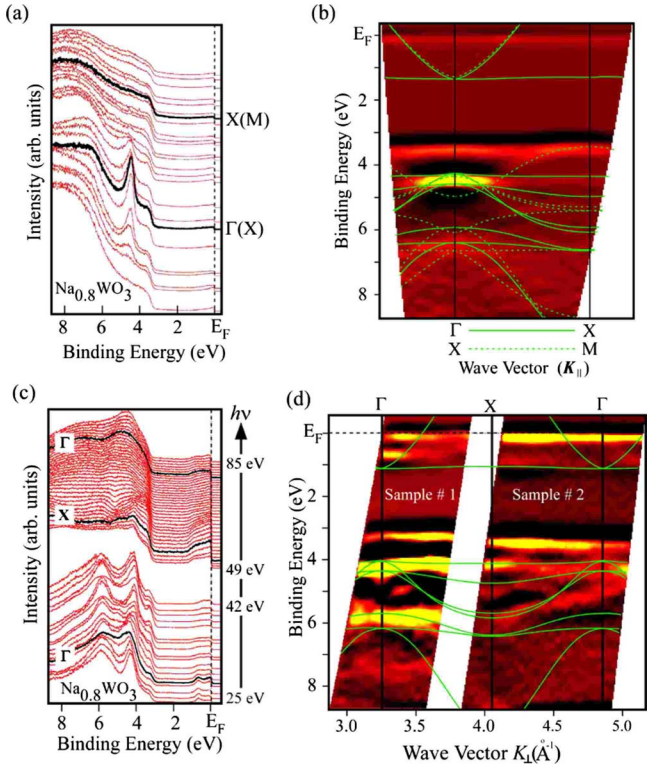

FIG. 2. (Color online) (a) Valence-band ARPES spectra of $Na_{0.8}WO_3$ measured along the $\Gamma(X)$-$X(M)$ (along $k_{\|}$) direction at low temperature. (b) Experimental valence-band structure obtained from ARPES experiment. The theoretical band calculation of $NaWO_3$ after shifting energy position of E_F is also shown by thin solid and dashed lines for comparison. (c) Normal-emission valence-band ARPES spectra of $Na_{0.8}WO_3$ measured at room temperature. Photon energy ($h\nu$) is denoted on spectra for two different samples. Samples 1 and 2 are measured from 25 to 42 eV and 49 to 85 eV, respectively. (d) Comparison of the experimental valence-band structure with the band calculation along $\Gamma(X)$ direction. Bright areas correspond to the experimental bands.

Figure 2(c) shows normal-emission ARPES spectra of $Na_{0.8}WO_3$ measured at room temperature from $h\nu$=25 to 85 eV. We have used photon energy from 25 to 42 eV for sample 1 and 49 to 85 eV for sample 2 in Elettra and Photon Factory synchrotron facilities, respectively. Since polarization of light sources are different for samples 1 and 2, the shape of spectra is somewhat different in these two measurements due to difference in the matrix-element term. The conduction band is clearly visible with a clear Fermi edge in this metallic compound. The valence band (around 3–8 eV) shows less-dispersive structures possibly due to momentum broadening along the $k_{\perp}$ direction. Nevertheless, we clearly observe three prominent features similar to Fig. 2(a). The most prominent feature at 4.0 eV shows symmetric behavior with respect to the spectra at $h\nu$=29 and 52 eV. This indicates that these photon energies correspond to high-symmetry points along $\Gamma(X)$ direction in BZ, namely, the Γ or X points. We have mapped out the experimental band structure as a function of $k_{\perp}$ as shown in Fig. 2(d). The momentum of photoelectron perpendicular to the surface is expressed by

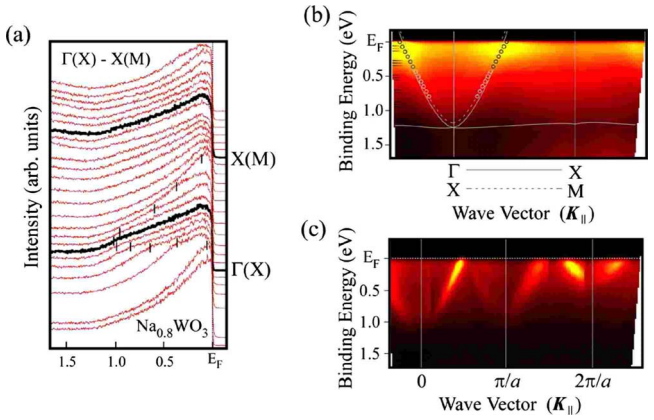

FIG. 3. (Color online) (a) ARPES spectra near E_F of $Na_{0.8}WO_3$ measured at low temperature along $\Gamma(X)$-$X(M)$ direction. Vertical bars are the guide for eyes of the band dispersion. (b) Experimental near-E_F band structure along $\Gamma(X)$-$X(M)$ direction for He-Iα (21.2 eV) photons. Theoretical band structure of $NaWO_3$ after shifting energy position of E_F is also shown by thin solid and dashed lines for comparison. (c) Similar band structure at 42 eV photons along the direction marked in Fig. 4(f) (white arrow mark, which is slightly away from the high-symmetry line), showing electronlike band around π/a.

$$k_{\perp} = \sqrt{\frac{2m}{\hbar^2}(E_{\text{kin}} \cos^2 \theta + V_0)}$$

where, E_{kin} is the kinetic energy of the photoelectron, V_0 is the inner potential, and θ is the emission angle of the photoelectron normal to the surface. The experimental band structure has been obtained by taking the second derivative of ARPES spectra and plotting the intensity as a function of $k_{\perp}$ and binding energy. From experimental band structure, we have determined the inner potential V_0 to be 15.3 eV which shows reasonable agreement with the periodicity of BZ and theoretical band calculation of $Na_{0.8}WO_3$. As reported earlier, the top of valence band at $\Gamma(X)$ point is not predicted in the band calculation and we explained that this apparently flat band may be dominated by the angle-integrated-type intensity/background from the strong intensity of the band at $M(R)$ point.[11] Our experimental ARPES results along the $k_{\perp}$ direction show a weakly dispersive nature at the top of the valence band. This suggests that the presence of intrinsic defects could be a possible origin of the observed band at $\Gamma(X)$ point. Earlier work on perovskite oxides[21] has shown that oxygen-vacancy states are induced at the top of the valence band, and these states are weakly dispersive. Hence we conclude that the oxygen vacancy in the system is possibly responsible for the evolution of density of states at the valence-band edge.

To investigate the conduction band in more detail, we measured ARPES spectra near E_F with the He-Iα photons at 14 K along $\Gamma(X)$-$X(M)$ high-symmetry line, and the results are shown in Fig. 3(a). We found a weak broad feature around 1.0 eV at $\Gamma(X)$ point, which disperses upward to form an electronlike pocket at $\Gamma(X)$ point. There is no signature of such feature at $X(M)$ point at this photon energy.

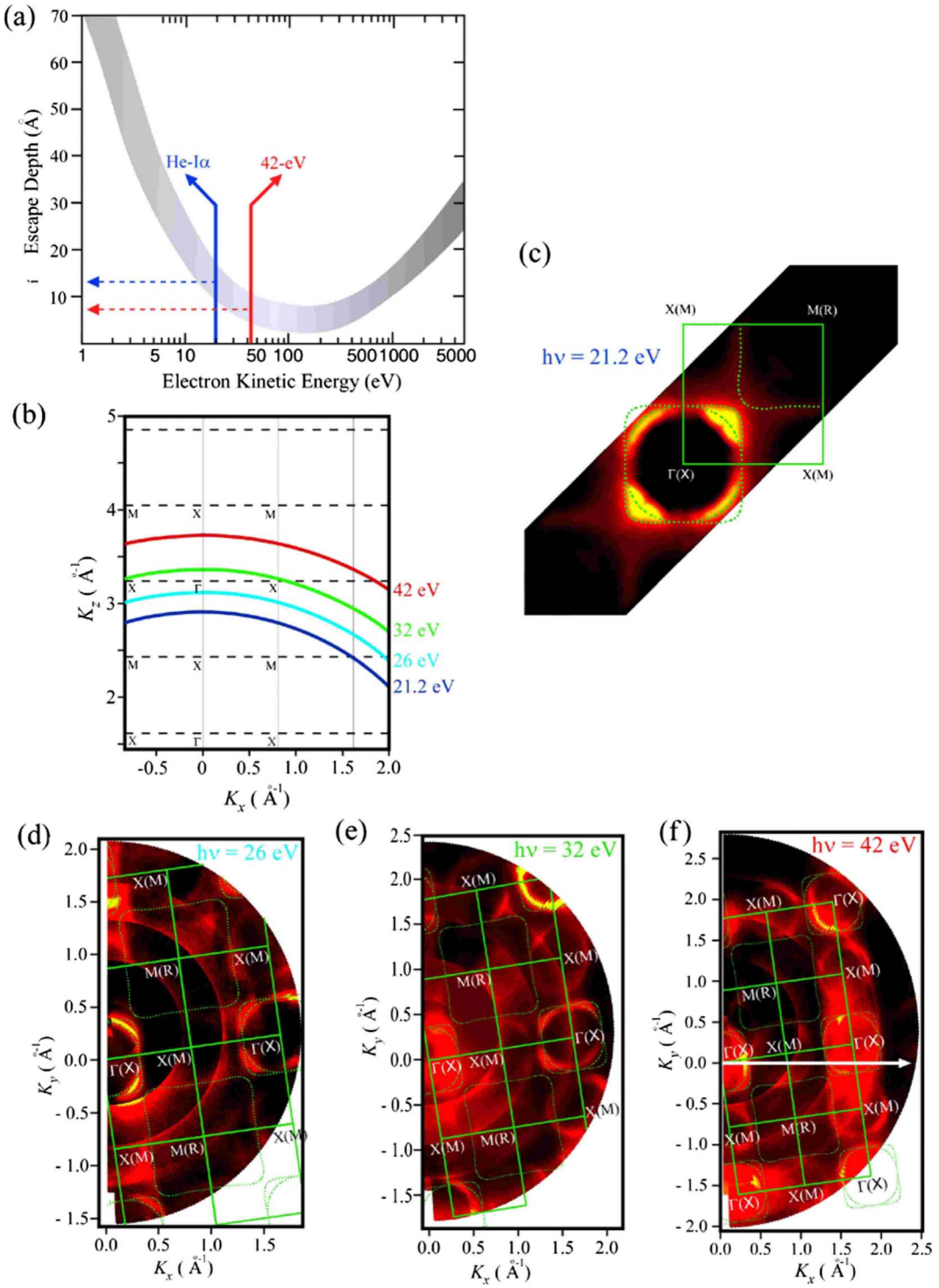

FIG. 4. (Color online) (a) Universal curve: electron escape depth as a function of their kinetic energy, (b) momentum position of ARPES cuts in k space for various photon energies. FSs of $Na_{0.8}WO_3$ for (c) the He-Iα (21.2 eV) line, (d) 26, (e) 32, and (f) 42 eV photons. FS shows an electronlike pocket at $\Gamma(X)$ point for the He-Iα photons, while similar electronlike pockets are also observed at $X(M)$ and $M(R)$ points with higher photon energies, likely due to the surface reconstruction. Dotted lines around $\Gamma(X)$ point are the calculated FSs (on ΓXMX and $XMRM$ plane) for fractional Na concentration based on the rigid-band model.

Surprisingly, we observe the Fermi edge throughout the BZ including around $X(M)$ point although its intensity is considerably weak. Such intensity would arise from the angle-integrated-type background due to the inelastically scattered electrons from the disordered site(s). Figures 3(b) and 3(c) show the plots of ARPES intensity near E_F with the He-Iα line and 42 eV photon energy, respectively. We find an electronlike pocket at $\Gamma(X)$ point, whose dispersion agrees satisfactorily with the band calculation. This band is assigned as the W $5d$ t_{2g} orbital from the band calculation. We find simi-

lar electronlike pockets at $X(M)$ point for 42 eV photons, in contrary to the band calculation. This would be due to the surface reconstruction, which we discuss later in FS mapping section. Interestingly, the reconstructed bands or FSs are not clearly observed for the He-Iα photons, implying that the He-Iα photons are more bulk sensitive than the 42 eV photons in $Na_{0.8}WO_3$.

To understand the differences between surface and bulk FS in $Na_{0.8}WO_3$, we have mapped out FS with different photon energies. From the universal curve [Fig. 4(a)], we infer that the electron escape depth slowly decreases from the He-Iα (21.2 eV) to 42 eV photon energy. Hence we mainly map from more bulk-sensitive FS to highly surface-sensitive FS with increasing photon energy from 21.2 to 42 eV. Figure 4(b) shows the momentum cut in k_z-k_x plane for k_y=0, where the ARPES intensity in Figs. 4(c)–4(f) were actually measured. We have used 21.2, 26, 32, and 42 eV photon energies for FS mapping, which are shown in Figs. 4(c)–4(f), respectively. Generally, two methods are used in ARPES to determine the location of FS. In the first method, we just follow the dispersion of bands from energy distribution curves (EDCs) and obtain the k-space point where the band actually crosses E_F. The FS of $Na_{0.8}WO_3$ excited by the He-Iα (21.2 eV) photons is obtained by this procedure, and the results are shown in Fig. 4(c). In the second method, the intensity at E_F is recorded with a series of azimuthal scans (ϕ), each step being repeated at different polar angles (θ) within a given photon energy. The FSs shown in Figs. 4(d)–4(f) are obtained by the second method. In all the experimental FS plots, the intensity is obtained by integrating the spectral weight within 30 meV with respect to E_F. We calculated the FS(s) (on ΓXMX and $XMRM$ plane) for fractional Na concentration in Na_xWO_3 at x=0.8, by assuming the rigid-band shift shown by dotted lines. We observe one spherical electronlike FS centered at the $\Gamma(X)$ point, which is covered with another squarelike FS. From Fig. 4(c), we find only one k_F point along the $\Gamma(X)$-$X(M)$ direction, while there are two distinct k_F points along the $\Gamma(X)$-$M(R)$ direction. These two Fermi surfaces are attributed to the W 5d t_{2g} bands which cross E_F. It is clearly seen that the FS at 21.2 eV photons [Fig. 4(c)] matches well with the theoretical prediction and there is no signature of the surface reconstruction, which suggests that obtained FSs centered at $\Gamma(X)$ point are of bulk origin. As soon as we move toward higher photon energy (i.e., 26–42 eV), we clearly recognize reconstructed spherical electronlike FS at $X(M)$ and $M(R)$ points, similar to the one at $\Gamma(X)$ point. The reconstructed FS is most clearly visible for 42 eV photons [Fig. 4(f)], which is supposed to be the most surface-sensitive photon energy in the range of photon energies in this study. It is noted that similar surface reconstruction at $X(M)$ and $M(R)$ points is also observed in insulating $Na_{0.025}WO_3$, even at 21.2 eV photons.[6] The rotation and deformation of the WO_6 octahedra in insulating $Na_{0.025}WO_3$ give rise to the orthorhombic crystal structure and that reflects strongly on its surface, giving rise to surface reconstruction even in relatively bulk-sensitive incident photon energy of 21.2 eV. Although the average crystal structure of bulk $Na_{0.8}WO_3$ derived from x-ray diffraction is cubic, we think that the structure of first few layers from the surface may be different due to reduced atomic coordinations, which may be responsible for the observed reconstructed FS or bands at $X(M)$ and $M(R)$ points. In insulating phase, the surface reconstruction at $M(R)$ point is stronger than $X(M)$ point whereas in metallic phase, it is found to be opposite. In Fig. 5, we show schematic view of the projection of two layers of WO_6 octahedra along (001) direction in bulk and surface of $Na_{0.8}WO_3$. In perovskite structure, two types of critical distortion would appear: (i) rotation of WO_6 octahedra, giving rise to tilted structures, and (ii) deformation of the individual WO_6 octahedra and/or displacement of the W atom from their central positions. We believe that, in bulk $Na_{0.8}WO_3$, there is no or very small distortion of WO_6 octahedra since the system has less disorder due to high doping of Na atom in WO_3 lattice, as shown in Fig. 5(a). On the other hand, the first few layers of $Na_{0.8}WO_3$ from the surface may deviate from the true bulk structure, and would show combined effect of rotation and deformation of WO_6 octahedra that gives rise to the $p(2\times2)$ superstructure at the surface [see Fig. 5(b)]. As a comparison with insulating $Na_{0.025}WO_3$, we believe that insulating phase has both $p(2\times2)$ and $c(2\times2)$ superstructures, which make the stronger intensity of FS at $M(R)$ point as compared to that at $X(M)$ point, although the effect of matrix-element difference between the spectra at both $X(M)$ and $M(R)$ points cannot be ignored to explain these differences. It is noted that similar FS/surface-reconstruction-derived bands were also found in the ARPES spectra of other system, Sr_2RuO_4.[22]

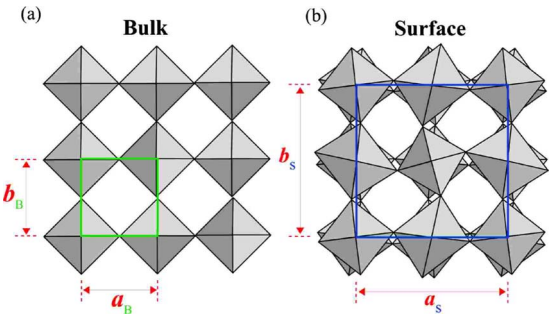

FIG. 5. (Color online) Projection of first two layers of WO_6 octahedra in (a) bulk and (b) surface of $Na_{0.8}WO_3$ along (001) direction. The combined effect of rotation and deformation of WO_6 octahedra gives rise to the superstructure at the surface of $Na_{0.8}WO_3$.

V. CONCLUSION

We have carried out high-resolution angle-resolved photoemission spectroscopy on $Na_{0.8}WO_3$ as a function of photon energy. We found that the top of the valence band at $\Gamma(X)$ point has no correspondence with the *ab initio* band calculation and possibly arises from the oxygen vacancy in the system. We found an electronlike band dispersion near E_F at $\Gamma(X)$ point, which is well described by the band calculation. The FS mapping with different photon energies indicates that

the electronic structure of first few layers from the surface is different from that of bulk, possessing new FSs at $X(M)$ and $M(R)$ points which are the replica of the FS at $\Gamma(X)$ point. The combined effects of rotation and deformation of WO_6 octahedra giving rise to the $p(2\times2)$ superstructure at the surface of $Na_{0.8}WO_3$ can well explain the reconstructed FS at $X(M)$ and $M(R)$ points found in more-surface-sensitive photons.

ACKNOWLEDGMENTS

This work was supported by grants from JSPS, JST-CREST, and the MEXT of Japan and that within India was supported by DST. The work at Elettra was supported by Indian DST and Italian MAE under the bilateral program of collaboration. S.R. acknowledges the financial support from JSPS.

*raj@arpes.phys.tohoku.ac.jp

†Also at Jawaharlal Nehru Centre for Advanced Scientific Research, Bangalore 560 054, India.

[1] C. G. Granqvist, *Handbook of Inorganic Electrochromic Materials* (Elsevier, Amsterdam, 1995).

[2] P. M. S. Monk, R. J. Mortimer, and D. R. Rosseinsky, *Electrochromism: Fundamentals and Applications* (VCH Verlagsgesellschaft, Weinheim, 1995).

[3] J. B. Goodenough, in *Progress in Solid State Chemistry*, edited by H. Reiss (Pergamon, Oxford, 1971), Vol. 5, pp. 145–399.

[4] H. R. Shanks, P. H. Slides, and G. C. Danielson, Adv. Chem. Ser. **39**, 237 (1963).

[5] A. S. Ribnick, B. Post, and E. Banks, Adv. Chem. Ser. **39**, 246 (1963).

[6] S. Raj, D. Hashimoto, H. Matsui, S. Souma, T. Sato, T. Takahashi, D. D. Sarma, P. Mahadevan, and S. Oishi, Phys. Rev. Lett. **96**, 147603 (2006).

[7] R. L. Benbow and Z. Hurych, Phys. Rev. B **17**, 4527 (1978).

[8] M. D. Hill and R. G. Egdell, J. Phys. C **16**, 6205 (1983).

[9] G. Hollinger, P. Pertosa, J. P. Doumerc, F. J. Himpsel, and B. Reihl, Phys. Rev. B **32**, 1987 (1985).

[10] T. Wolfram and L. Sutcu, Phys. Rev. B **31**, 7680 (1985).

[11] S. Raj, D. Hashimoto, H. Matsui, S. Souma, T. Sato, T. Takahashi, S. Ray, A. Chakraborty, D. D. Sarma, P. Mahadevan, W. H. McCarroll, and M. Greenblatt, Phys. Rev. B **72**, 125125 (2005).

[12] S. Raj, H. Matsui, S. Souma, T. Sato, T. Takahashi, A. Chakraborty, D. D. Sarma, P. Mahadevan, S. Oishi, W. H. McCarroll, and M. Greenblatt, Phys. Rev. B **75**, 155116 (2007).

[13] H. R. Shanks, J. Cryst. Growth **13-14**, 433 (1972).

[14] B. W. Brown and E. Banks, J. Am. Chem. Soc. **76**, 963 (1954).

[15] P. E. Blöchl, Phys. Rev. B **50**, 17953 (1994).

[16] G. Kresse and D. Joubert, Phys. Rev. B **59**, 1758 (1999).

[17] G. Kresse and J. Furthmüller, Phys. Rev. B **54**, 11169 (1996); Comput. Mater. Sci. **6**, 15 (1996).

[18] V. N. Strocov, H. I. Starnberg, P. O. Nilsson, H. E. Brauer, and L. J. Holleboom, Phys. Rev. Lett. **79**, 467 (1997).

[19] V. N. Strocov, Int. J. Mod. Phys. B **9**, 1755 (1995).

[20] V. N. Strocov, H. I. Starnberg, and P. O. Nilson, J. Phys.: Condens. Matter **8**, 7539 (1996).

[21] N. Shanthi and D. D. Sarma, Phys. Rev. B **57**, 2153 (1998).

[22] R. Matzdorf, Z. Fang, Ismail, J. Zhang, T. Kimara, Y. Tokura, K. Terakura, and E. W. Plummer, Science **289**, 746 (2000).